On the global dynamics of chatter in the orthogonal cutting model

Zoltan Dombovari, David A.W. Barton, R. Eddie Wilson, Gabor Stepan

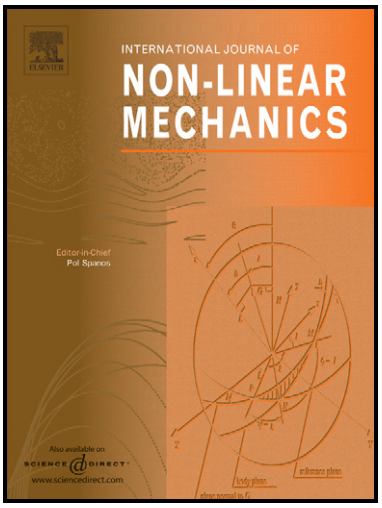

www.elsevier.com/locate/nlm

On the global dynamics of chatter in the orthogonal cutting model

Zoltan Dombovari, David A.W. Barton, R. Eddie Wilson, Gabor Stepan

PII: S0020-7462(10)00149-6
DOI: doi:10.1016/j.ijnonlinmec.2010.09.016
Reference: NLM 1772

To appear in: *International Journal of Non-Linear Mechanics*

Received date: 4 December 2009
Revised date: 15 September 2010
Accepted date: 26 September 2010

Cite this article as: Zoltan Dombovari, David A.W. Barton, R. Eddie Wilson and Gabor Stepan, On the global dynamics of chatter in the orthogonal cutting model, *International Journal of Non-Linear Mechanics*, doi:10.1016/j.ijnonlinmec.2010.09.016

On the Global Dynamics of Chatter in the Orthogonal Cutting Model

Zoltan Dombovari[*,a,c], David A.W. Barton[b], R. Eddie Wilson[b], Gabor Stepan[a]

[a] *Department of Applied Mechanics, Budapest University of Technology and Economics, Budapest, H-1521, Hungary*
[b] *Department of Engineering Mathematics, University of Bristol, Bristol, BS8 1TR, United Kingdom*
[c] *Department of Mechanical Engineering, Ideko-Danobat Group, Elgoibar, Gipuzkoa 20870, Spain*

Abstract

The large-amplitude motions of a one degree-of-freedom model of orthogonal cutting are analysed. The model takes the form of a delay differential equation which is non-smooth at the instant at which the tool loses contact with the workpiece, and which is coupled to an algebraic equation that stores the profile of the cut surface whilst the tool is not in contact. This system is approximated by a smooth delay differential equation without algebraic effects which is analysed with numerical continuation software. The grazing bifurcation that defines the onset of chattering motion is thus analysed as are secondary (period-doubling etc.) bifurcations of chattering orbits, and convergence of the bifurcation diagrams is established in the vanishing limit of the smoothing parameters. The bifurcation diagrams of the smoothed system are then compared with initial value simulations of the full non-smooth delay differential algebraic equation. These simulations mostly validate the smoothing technique and show in detail how chaotic chattering dynamics emerge from the non-smooth bifurcations of periodic orbits.

Key words: orthogonal cutting, delay differential equation, differential algebraic equation, non-smooth, chatter, fly-over

1. Introduction

In the machining industry it is well known that at high material removal rates, turning, milling and drilling processes are subject to chattering motions in which the tool repeatedly loses and re-establishes contact with the workpiece. Chattering results in a very poor quality finish, see figure 1(*a*), so in practice the need to avoid it limits the material removal rate and places bounds on the technological parameters such as the spindle speed and the depth of cut (also known as the chip width). These bounds are in addition to those due to the power and torque characteristics of the machine.

The general aim of this paper is to understand in more detail the dynamical mechanisms involved in the onset of chattering in turning processes, where a quasi-stationary tool cuts into a rapidly rotating workpiece. To simplify matters, we restrict our analysis to the special case of *orthogonal cutting*, depicted in figure 2.

In turning processes, the cutting force between the tool and the workpiece is a function of the chip thickness, that is, the difference between the tool position and the surface position. The surface position was determined one (or more) revolutions earlier by the tool's past motion. Turning processes are thus *regenerative* [1, 2] in the sense that the tool's motion is forced by its own history, leading to models based on delay differential equations (DDEs). These models admit equilibria corresponding to steady cutting, where the chip thickness is independent of time, but the stability of this regime is not assured. By analysing when steady cutting is linearly unstable, we may thus identify combinations of technological parameters which the machinist should avoid [3–10].

In practice, the stability of the process is complicated by nonlinear effects, and the typical situation is indicated by the one-dimensional bifurcation diagram in figure 1(*b*), where we fix the spindle speed and analyse the dynamics of the tool as the chip width is varied. Here $\|x\| := \max_t x(t) - \min_t x(t)$ denotes the peak-to-peak magnitude of the tool's motion $x(t)$, so that on branch A, where $\|x\| = 0$, we have linearly stable steady cutting in which the chip thickness is constant. As the chip width is increased, steady operation becomes linearly unstable at the Hopf bifurcation point B. However, normal form computations [11, 12] and measurements [13, 14] show that the bifurcation is subcritical, indeed robustly so over a wide range of parameters and cutting force characteristics [15]. Hence the branch C of periodic orbits that emanates 'bends back' and the periodic orbits on it are themselves unstable and hence are not observable in experiments.

However, we know from experiments [13, 16] that complicated large amplitude chattering motions E (figure 1(*b*)) are possible at depths of cut less than that of the Hopf bifurcation point. Hence in regime 2, there is bistability in that sufficiently large perturbations to steady cutting can result in sustained chattering oscillations [13]. In contrast, in regime 1, only steady cutting is possible and in regime 3, only chattering is possible. Qualitatively this type of behaviour is seen in many different engineering applications, for example, pipe-flow [17].

The focus of this paper is the vicinity of the point D marked in figure 1(*b*). Specifically, we shall examine how the unsta-

[*]Corresponding author
Email addresses: dombo@mm.bme.hu (Zoltan Dombovari), david.barton@bristol.ac.uk (David A.W. Barton), re.wilson@bristol.ac.uk (R. Eddie Wilson), stepan@mm.bme.hu (Gabor Stepan)

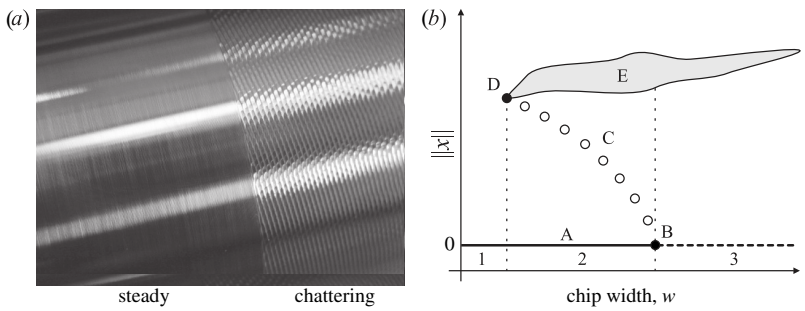

Figure 1: Panel (*a*) shows a photograph of a machined workpiece. The smooth surface to the left was produced by steady cutting, whereas to the right we may observe so-called *sunflower spirals* which are a typical result of tool chatter (photograph provided by Ideko). Panel (*b*) depicts a schematic bifurcation diagram showing typical dependence of the tools motion on the chip width w. Here solid / dashed lines represent respectively stable / unstable steady-state cutting. From the Hopf point B an unstable period-one branch marked C emerges. Our interest is in point D, which denotes the onset of chattering motions at E.

ble branch C connects to stable chattering motions in region E, and how the complexity of these motions develops through secondary bifurcations. The simplest mechanism for a periodic branch to regain stability is via a cyclic fold / SNLS (Saddle Node of a Limit Cycle) bifurcation, and we show that indeed this is the mechanism at D, albeit a non-smooth variant where the branch C turns back at the instant its orbits attain sufficient amplitude for the tool to leave the workpiece. This non-smooth fold point has a rather intricate structure of accumulating branches which may be detected by following through sequences of further (non-smooth) fold and (smooth) period doubling bifurcations. See the monograph [18] for a recent account of non-smooth bifurcation theory.

To analyse these solution structures, our chief weapon is numerical continuation software, which is a well established technique for investigating dynamical systems. The key idea is that one may trace out branches of solutions (which may be equilibria or periodic orbits) as a parameter is varied without resorting to repeated solution of the initial value problem. In particular, branches of unstable solutions may be followed which subsequently bifurcate to produce stable dynamics, so that competing stable behaviours can be identified efficiently without an exhaustive search of the initial value and parameter spaces. The theoretical foundations of numerical continuation were developed in the 1980s (see for example [19–21] for an overview), and well-known packages include AUTO [22] and MatCont [23] for ordinary differential equations (ODEs). The analysis of DDEs, such as arise from regenerative processes, is complicated by the infinite dimensional state space, but these problems may be tackled by more sophisticated packages such as DDE-BIFTOOL [24] (which we use) and PDDE-CONT [25].

Unfortunately, numerical continuation depends upon continuous differentiability of the model with respect to its solutions and parameters, and our model for cutting is non-smooth at the instant when the tool loses contact with the workpiece. Furthermore, the tool position and its history are not sufficient to close the initial value problem for chattering motions. This is because when the tool is flying (i.e., has lost contact with the workpiece) a separate variable must be maintained to store the surface height of the workpiece for future computation after the tool has landed. This switch gives rise to a combined differential-algebraic system.

The key achievements of this paper are thus two-fold: 1) a smooth approximation to the cutting model, with no algebraic effects, is developed which may then be analysed with the DDE-BIFTOOL package, and 2) the bifurcation structure of the smooth approximation is elucidated and related to that of the non-smooth model, and, in particular, we show that the onset of chattering is via a type of non-smooth fold point.

The remainder of the paper is structured as follows. In section 2 we develop and parametrise a regenerative one degree-of-freedom model for orthogonal cutting, which is generalised to incorporate non-smooth and algebraic effects due to the tool leaving the workpiece. In section 3 we then describe how the model may be smoothed for computational purposes, and we show convergence of the bifurcation diagrams in the limit of vanishing smoothing parameters that demonstrate unequivocally that point D is a non-smooth cyclic fold. Then in section 4, we probe the secondary bifurcation sequences and the stable chattering behaviour in more detail and show how these correspond to numerical simulations of the initial value problem. Then section 5 presents conclusions.

2. Model description

In this section, a simple model is developed for the orthogonal cutting process that can demonstrate chattering behaviour. The model is formulated as a delay differential algebraic equation (DDAE) and includes the regenerative effect of turning processes and the non-smoothness when contact between the cutting tool and the workpiece is lost.

2.1. Permanent contact model

We begin by modelling the simple case where the tool is in permanent contact with the workpiece [15]. As we have described, turning processes have a so-called *regenerative effect* or memory property: when the tool is in permanent contact with

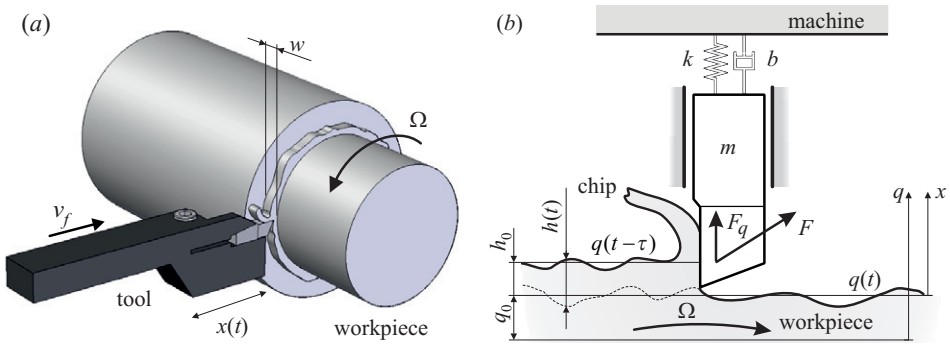

Figure 2: Panel (*a*) shows a schematic of the cutting tool in contact with the workpiece. The workpiece is rotating with angular velocity Ω and the tool enters the workpiece with feed velocity $v_f = h_0\Omega/(2\pi)$. Panel (*b*) is a graphical representation of the model (2) where the forces on the cutting tool are proportional to the chip thickness $h(t) = q(t-\tau) - q(t) + h_0$, where $\tau = 2\pi/\Omega$ is the period of revolution.

the workpiece, the thickness of the chip that is cut is the difference between the current position of the cutting tool and the position of the cutting tool one revolution earlier. Consequently, this introduces a delay of time $\tau = 2\pi/\Omega$ into the system, where Ω is the spindle speed. If $q(t)$ denotes the displacement of the tool orthogonal to the workpiece, then the instantaneous chip thickness $h(t)$ is given by

$$h(t) = q(t-\tau) - q(t) + h_0 = \Delta h(t) + h_0, \tag{1}$$

where h_0 is the desired steady-state chip thickness (proportional to the feed rate), see figure 2(*b*).

We consider a one degree-of-freedom model of the motion of the cutting tool-toolholder-machine system as illustrated in figure 2(*b*). In the direction perpendicular to the workpiece the equation of motion is

$$\ddot{q}(t) + 2\kappa\omega_n\dot{q}(t) + \omega_n^2 q(t) = \frac{1}{m}F_q, \tag{2}$$

where $q(t)$ is the position of the cutting tool relative to the tool holder that provides the constant feed, which is just h_0 for one revolution of the workpiece. The system parameters are the natural angular velocity ω_n, the damping ratio κ and the modal mass m. Here F_q is the orthogonal component of the cutting force which must be determined empirically. In practice, we find F_q is linearly proportional to the chip width (depth of cut) w, but depends nonlinearly on the chip thickness $h(t)$. Via (1), it follows that (2) is a DDE. Throughout the paper we fix $\kappa = 0.04$ as a representative damping ratio.

The classical approximation to F_q is given by the three-quarter rule $F_q \sim wh^{3/4}$, see [26], which has infinite gradient at $h = 0$ when the tool leaves the workpiece. To avoid this degeneracy, we use instead the approximation due to Shi and Tobias [13], which takes the cubic polynomial form

$$F_q(h(t)) = w(\rho_1 h(t) + \rho_2 h^2(t) + \rho_3 h^3(t)), \tag{3}$$

with typical measured parameter values $\rho_1 = 6109.6\,\mathrm{N\,mm^{-2}}$, $\rho_2 = -54141.6\,\mathrm{N\,mm^{-3}}$ and $\rho_3 = 203769\,\mathrm{N\,mm^{-4}}$ for steel.

We consider tool motion $x(t)$ relative to the equilibrium position $q_0 = F_q(h_0)/m\omega_n^2$, and rescale time and displacement using the natural angular velocity ω_n and the desired chip thickness h_0 respectively, so that

$$\tilde{t} = \omega_n t, \quad \tilde{x} = x/h_0,$$
$$\tilde{w} = w\frac{\rho_1 + 2\rho_2 h_0 + 3\rho_3 h_0^2}{m\omega_n^2}, \quad \tilde{\tau} = \omega_n\tau, \quad \tilde{\Omega} = \frac{2\pi}{\tilde{\tau}} = \Omega/\omega_n,$$
$$\eta_2 = \frac{h_0(\rho_2 + 3\rho_3 h_0)}{\rho_1 + 2\rho_2 h_0 + 3\rho_3 h_0^2} \quad \text{and} \quad \eta_3 = \frac{h_0^2\rho_3}{\rho_1 + 2\rho_2 h_0 + 3\rho_3 h_0^2}, \tag{4}$$

where the dimensionless cutting force parameters become $\eta_2 = -0.20015$ and $\eta_3 = 0.01946$. (These parameters are typical for finishing-type operations where surface quality is important.) Thus (2) may be rewritten in the canonical non-dimensional form

$$x''(t) + 2\kappa x'(t) + x(t) = F(\Delta h(t)) = w(\Delta h(t) + \eta_2\Delta h^2(t) + \eta_3\Delta h^3(t)), \tag{5}$$

where the tildes are dropped for clarity. Here $\Delta h(t) := h(t) - 1 = x(t-\tau) - x(t)$ is the (non-dimensional) instantaneous chip thickness.

2.2. *Non-smooth intermittent contact model*

We now consider how to augment model (5) to include motions where the tool loses contact with the workpiece. At the instant that contact is first lost, the chip thickness attains zero and the cutting force is 'switched off' until the tool regains contact. In consequence, the definition of the cutting force is augmented with $F(h) = 0$ for $h < 0$, and thus it is not differentiable at $h = 0$.

Furthermore, since the original equation of motion (5) tracks only the position of the cutting tool and not the surface of the workpiece, equation (1) defining the chip thickness becomes invalid once contact is lost. Thus we introduce the surface height function $\chi(t)$ defined by the recurrence relation

$$\chi(t) = \begin{cases} x(t), & \text{if cutting,} \\ \chi(t-\tau) + 1, & \text{if flying,} \end{cases} \tag{6}$$

where $x(t)$ is the position of the cutting tool from (5). Clearly, when the cutting tool is in contact with the surface, the positions of the two are identical. However, when the cutting tool

is not in contact, the surface height is simply the same as it was one revolution earlier, corrected by the (non-dimensionalised) feed-rate. Consequently, the new expression for chip thickness becomes

$$h(t) = \chi(t-\tau) - x(t) + 1 = \Delta h(t) + 1. \tag{7}$$

In summary, the final non-smooth model is a DDAE defined by (5), (6) and (7). For convenience we define the cutting and flying vector-fields $\mathcal{S}_\mathrm{c}$ and $\mathcal{S}_\mathrm{f}$ respectively in the form

$$\mathcal{S}_\mathrm{c}(t) = \begin{bmatrix} x'(t) \\ F(\Delta h(t)) - 2\kappa x'(t) - x(t) \\ x(t) - \chi(t) \end{bmatrix} \tag{8}$$

and

$$\mathcal{S}_\mathrm{f}(t) = \begin{bmatrix} x'(t) \\ -2\kappa x'(t) - x(t) \\ \chi(t-\tau) + 1 - \chi(t) \end{bmatrix}, \tag{9}$$

so that the full model may be summarised by

$$\begin{bmatrix} x'(t) \\ x''(t) \\ 0 \end{bmatrix} = H(h(t))\mathcal{S}_\mathrm{c}(t) + [1 - H(h(t))]\mathcal{S}_\mathrm{f}(t), \tag{10}$$

where H is the Heaviside step function. The (infinite dimensional) phase-space of (10) is given by $(x_t(s), x'_t(s), \chi_t(s))$ for $s \in [-\tau, 0]$, where $(\cdot)_t(s) = (\cdot)(t+s)$, and consequently solutions of the model must be projected onto a two-dimensional surface in order to be visualised. In the analysis that follows we shall speak of the *switching surface*, defined to be the set of all states where the *switching condition* $h(t) = 0$ is satisfied, and thus where (10) switches between the cutting and flying vector fields.

3. Smoothed equations

We now approximate the non-smooth system (10) of DDAE with a smoothed delay differential equation DDE approximation, so that even chattering motions may be analysed by the standard numerical continuation package DDE-BIFTOOL. We then demonstrate continuation computations and study their convergence in the smoothing parameters. In particular, we study the nature of the onset of chattering motions (point D in figure 1(*b*)) and verify that this a type of non-smooth fold.

3.1. Smoothed intermittent contact model

Firstly, in (10), we may approximate the Heaviside step function with the smooth function

$$H(h(t)) \approx H_{\varepsilon_1}(h(t)) := \frac{1}{2}\left(1 + \tanh\frac{h(t)}{\varepsilon_1}\right), \tag{11}$$

where $\varepsilon_1 > 0$ is a smoothing parameter, so that we expect to recover the full non-smooth dynamics in the limit $\varepsilon_1 \to 0$.

Secondly, we must address the more serious difficulty in (10), namely the algebraic recursion, which cannot be tackled by standard numerical continuation packages. Our approach is to approximate (6) by a differential equation by introducing a further smoothing in the form of the singular perturbation $\varepsilon_2\chi'(t)$ ($\varepsilon_2 > 0$) in the third component of (10). The fully smoothed DDE approximation thus takes the form

$$\begin{bmatrix} x'(t) \\ x''(t) \\ \varepsilon_2\chi'(t) \end{bmatrix} = H_{\varepsilon_1}(h(t))\mathcal{S}_\mathrm{c}(t) + [1 - H_{\varepsilon_1}(h(t))]\mathcal{S}_\mathrm{f}(t), \tag{12}$$

where χ is now a *fast* variable that tracks either $x(t)$ or $\chi(t-\tau)+1$ with the characteristic time scale ε_2.

The choice of the smoothing parameters ε_1 and ε_2 is critical and we experiment with them later in section 3.3. In particular, they must be chosen sufficiently small so as to avoid introducing dynamical artefacts which are solutions of (12) but not of (10). However, pathologically small choices will result in unnecessarily long computations.

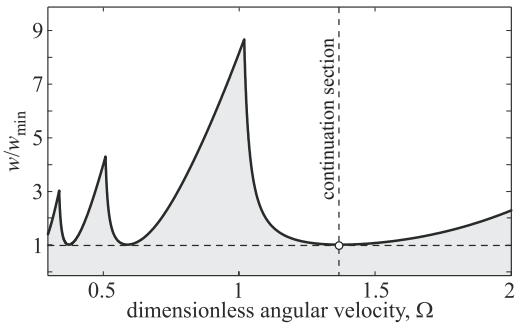

Figure 3: Two-parameter bifurcation diagram of the steady-state cutting. The black curve represents a Hopf bifurcation curve; along this curve the bifurcations are subcritical. Consequently, there are unstable periodic orbits coexisting with the stable steady-state cutting solutions in the grey region of the diagram.

3.2. Method of numerical investigation

To investigate the dynamics of the system, we perform one-parameter continuations in the chip width w, with all other parameters held constant, in order to compute the structure sketched in figure 1(*b*). In each computation, we begin with the trivial solution $x(t) \equiv 0$ and follow the branch of unstable periodic orbits that emanates from the subcritical Hopf bifurcation. These calculations are at first entirely smooth, since the oscillations represent small amplitude motions in which the tool does not leave the workpiece, and which can be followed [15] using the basic model (5). However, as the amplitude of the unstable periodic orbit grows, then it begins to incorporate motion in which the tool flies, for which the full model (10) and its smoothing (12) are required.

Note that linear stability analysis of the steady cutting solution $x \equiv 0$ leads to the well-known *lobe* structure in the Ω–w stability chart [1–3, 11, 15, 27], see figure 3. In this paper, we focus on computations which cut the 'first' lobe at its minimum with respect to w, for which the non-dimensional spindle speed Ω is highest, indicated by the vertical section in figure 3. (For the choice of physical parameters we have adopted in section 2,

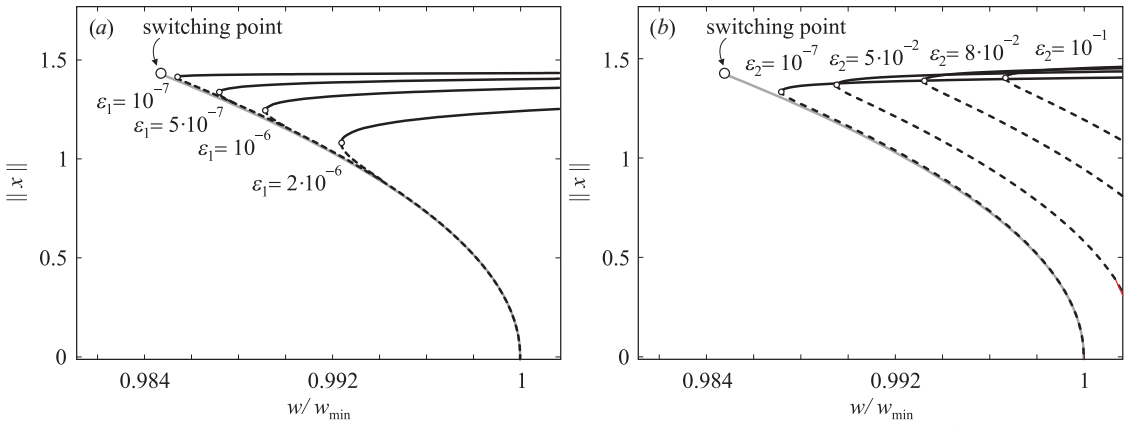

Figure 4: The panels show a series of one-parameter continuations (bold curves) of the smoothed model (12) in the vicinity of the fold-type point at which the branches turn over. The grey curve indicates a continuation of the unstable periodic orbit of the basic model (5) which captures motions with no loss of contact, and the large circle on this branch denotes the switching point at which zero chip thickness is attained. In panel (*a*) we fix $\varepsilon_2 = 10^{-7}$ and reduce ε_1, and in (*b*) we fix $\varepsilon_1 = 5 \cdot 10^{-7}$ and reduce ε_2. In these limits, the unstable portion of the branches accumulate on the branch for (5), and the fold points accumulate on the switching point for (5) if ε_1 is reduced sufficiently.

we thus have $\Omega \simeq 1.37$.) In all plots we then present the chip width normalised by its minimum value $w_{\min}$ at the Hopf bifurcation.

Preliminary computations (not presented here) indicate similar bifurcation structure for other constant Ω sections. Some of this similarity can be explained by the standard DDE invariance property, which relates the lobes to each other. Specifically, if we have a periodic orbit $\phi(t)$ with period T for a particular time delay $\tau = \tau_0$, then $\phi(t)$ is also a periodic orbit for time delay $\tau = \tau_0 + nT$ where $n = 1, 2, \ldots$. However, stability properties are not preserved by this transformation. In consequence, whereas the secondary bifurcations of the continuation through the first lobe include many period doubling bifurcations, the continuations through other lobes typically involve Neimark-Sacker bifurcations giving rise to quasi-periodic oscillations which cannot be continued further by DDE-BIFTOOL.

3.3. Effect of the smoothing parameters

We now follow the continuation procedure described in section 3.2, in order to investigate the dynamics of the smoothed system (12). Of particular interest is the choice of the smoothing parameters, ε_1 and ε_2, and how small they must be chosen for the dynamics of the non-smooth model (10) to be reproduced robustly. Furthermore, we wish to establish the nature of the transition to chattering dynamics, at point D in figure 1(*b*). These questions are the focus of figure 4, which summarises our results.

Figure 4 establishes two things. Firstly, as ε_1 and ε_2 are reduced towards zero, there is an accumulation in the branches computed from the smoothed model (12). In fact, this accumulation establishes only the self-consistency of the smoothed model, and not that it reproduces the dynamics of the full model (10) — a point that we will return to in section 4.

Secondly, figure 4 shows that the branch of unstable periodic orbits emanating at the Hopf bifurcation 'turns over' in a cyclic fold (Saddle Node of a Limit Cycle) at which it regains stability. The location of this fold may then be examined as ε_1 and ε_2 are successively reduced. When this limiting process is followed, we find that the fold for the smoothed model (12) tends to the point at which the orbits of the permanent contact model (5) attain loss of contact between the tool and the workpiece.

In consequence, it seems that we have established the nature of the point D in figure 1(*b*). The limiting behaviour of the smoothed model indicates that the branch of unstable periodic orbits of the full non-smooth model (10) regains stability via a non-smooth cyclic fold, at which point its orbits simultaneously lose contact between the tool and the workpiece. This is a well-known type of grazing bifurcation [18, Chapter 7]. However, as we shall now see, a detailed investigation of the secondary bifurcation structure beyond the fold point reveals a more complicated situation.

4. Details of chattering dynamics

We now extend our analysis to a more detailed study of chattering motions — that is the region denoted E in figure 1(*b*). There are two components in this work.

- Firstly, in section 4.1, we extend our numerical continuation of the smoothed model (12) to consider secondary bifurcations that occur beyond the fold point that we have already examined. In summary, we discover a complicated bifurcation structure in which many branches of period doubled orbits also accumulate at the fold point, but 'from the right' in the sense of figure 4. This result indicates that the onset of chattering motion is not via a simple grazing cyclic fold, and that initial chattering motions are probably not simple periodic orbits.

- Thus secondly, in section 4.2, we perform time-domain simulations of the full non-smooth model (10) in order

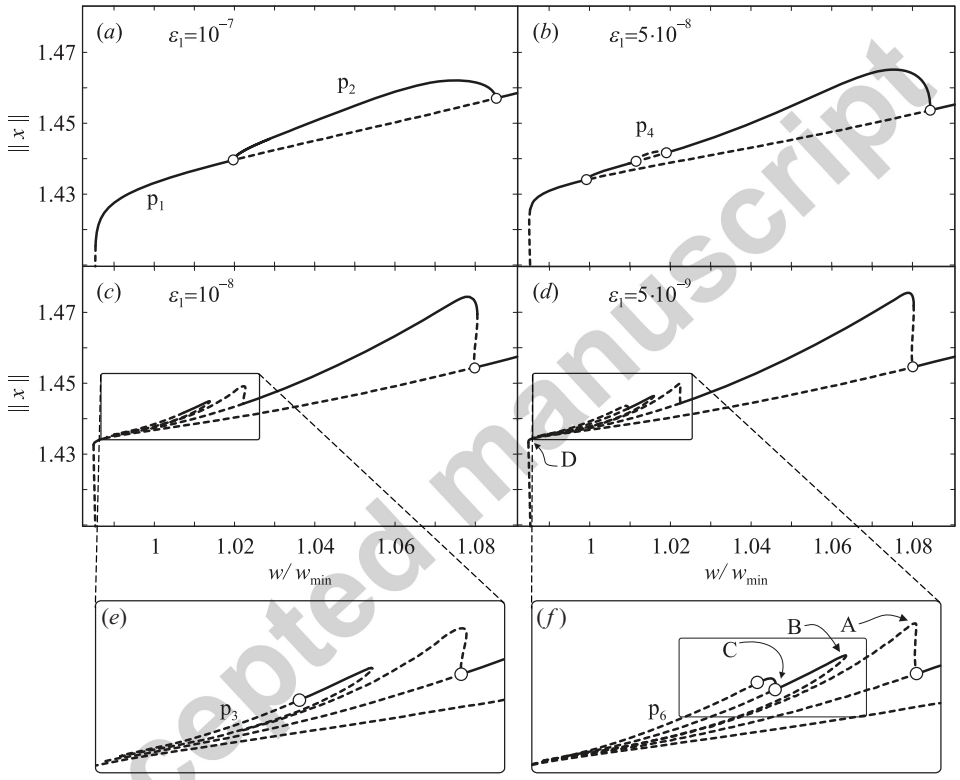

Figure 5: Panels (*a*)–(*d*) show the convergence of the bifurcation structure of the smoothed model (12) as $\varepsilon_1 \to 0$. Throughout we fix $\varepsilon_2 = 10^{-7}$. In (*a*) there are two period-doubling bifurcations connected by a branch of period-two orbits. As ε_1 is decreased a 'bubble' of period-four orbits emerges as shown in (*b*). Panels (*c*) and (*d*) appear to show the converged bifurcation structure. All of the left-hand period-doubling bifurcations have moved towards the fold point, which suggests that all the branches shown actually emerge from the grazing bifurcation in the non-smooth model (cf. the labelled point D). Isolated branches of period-three and period-six orbits, connected by a period-doubling bifurcation at point C, are shown in (*c*) and (*d*) respectively.

to eliminate artefacts due to the smoothing process. In summary, we establish that there is an immediate 'jump' to chaotic dynamics, and we trace out how the dynamics evolve as the chip width is increased, demonstrating the correspondence between periodic windows in the time simulation and stable sections of periodic orbit in the numerical continuation.

4.1. Numerical continuation and secondary bifurcations

We now follow on from figure 4 to continue branches of periodic orbits to the smoothed model (12), as the chip width w is increased beyond the non-smooth fold point. In particular, we focus on computing secondary bifurcations and the branches that emanate from them. Our experience with computations of the smoothed model indicates that qualitative dynamics are relatively robust to the choice of the smoothing parameter ε_2, but the choice of ε_1 is critical. Hence throughout we fix $\varepsilon_2 = 10^{-7}$ and consider a sequence of computations as ε_1 is reduced. Figure 5 summarises the results.

Further continuation of the branches shown in figure 4 for $\varepsilon_1 = 10^{-7}$ demonstrates the opening up of a stable period-doubled bubble, as seen in figure 5(a). However, as ε_1 is decreased further, see figure 5(b), a second stable period-doubled bubble emerges so as to introduce a window of unstable period-four orbits. Moreover, the original left-hand period-doubling bifurcation has moved towards the fold. This process continues in figure 5(c) and (d) as ε_1 is reduced further and we begin to recover the converged bifurcation structure of the model. In short we discover an apparent cascade of period-doubling bifurcations, where the left-hand bifurcation of each new bubble approaches the fold point as ε_1 is successively reduced.

Furthermore, as ε_1 is decreased, the criticality of the period-doubling bifurcations changes from supercritical to subcritical. The change in criticality introduces additional cyclic fold bifurcations into the branch structure, labelled A and B in figure 5. It appears that, in the limit of $\varepsilon_1 \to 0$, these cyclic folds also become non-smooth fold points. However, no further bifurcating branches are found to emerge from these extra non-smooth fold points. The change in criticality is further highlighted in figure 6 which shows the change in the period-3 and period-6 branches as ε_1 is changed from $5 \cdot 10^{-9}$ to 10^{-9}.

In consequence, it seems the onset of *stable* periodic chattering motion at the primary fold point, discovered in section 3.3, is an artefact of the smoothing process. Instead, it seems that the fold point is a more complicated type of grazing bifurcation from which infinitely many branches of *unstable* periodic orbits emanate. This is reminiscent of the 'Big Bang bifurcation' of Avrutin and Schanz [28] and as such we label this point B^3. The emerging periodic orbits are then absorbed at period-doubling bifurcations at larger values of the chip width parameter. In fact, a more detailed investigation also reveals the emanation of branches of unstable period-three and period-six orbits which do not connect with the period-one/two/four structure (other than at the fold point) but which can be readily be found by numerical simulation and then continued.

This bifurcation structure, consisting of an infinite accumulation of unstable periodic orbits, has been discovered in simpler non-smooth dynamical systems [18, see examples in Chapter 7] and is associated with the instantaneous onset of localised chaotic dynamics. However, a recent parallel study [29] which works directly on the non-smooth model (10), demonstrates that the period doubling cascade is an artefact of the smoothing, and that only the first two right-most period-doubling bifurcations, see figure 5(b), persist in the perfectly non-smooth model. The $\varepsilon_1, \varepsilon_2 \to 0$ limiting process thus has features which we could not explore fully from mathematical perspective, but the results obtained so far are also supported by the time-domain simulations of the limiting case.

4.2. Time-domain simulations

To establish the validity of the smoothed model (12) we resort to numerical simulation of the full non-smooth model (10). If the smoothed model is an accurate representation of the non-smooth model, then there should be good agreement between the results away from any non-smooth grazing bifurcations. Furthermore, we present the results for numerical simulations of the smoothed model (12) to enable a complete comparison of the results.

Moreover, while numerical simulation cannot provide the full bifurcation structure of the model, it will reveal any chaotic attractors in the system which cannot be studied directly using numerical continuation methods. Thus numerical continuation and numerical simulation are complementary to each other in elucidating the dynamics of a model.

To integrate (10) the Matlab routines dde23 and ode45 are used alternately to integrate the DDE and ODE parts of the system respectively; the built-in event detection features of the Matlab routines enable the switching points to be found to machine precision (since the switch is defined by an algebraic equation), thus the accuracy of the integration is unaffected by the switching. The algebraic constraint is implicitly incorporated into the system through modifications to the initial function segment provided to dde23. At each parameter value, (10) is integrated for 1000 non-dimensional time units and the first 200 time-units of data are then discarded to account for the transient behaviour. The output of each simulation run is used as the initial condition for the next simulation run.

Figure 8 shows results from numerical simulations of (10) overlaid with the cloud from numerical continuation of (12). As suggested by the numerical continuation results, the primary fold point / grazing bifurcation acts as an organising centre for the dynamics.

The values on the vertical axis of figure 8 are defined by

$$\xi := \mathrm{sgn}(x(t)) \sqrt{x(t)^2 + x(t-\tau)^2}, \tag{13}$$

at the point the orbit intersects the Poincaré section

$$\Pi := \{x(t) + x(t-\tau) = 0\}. \tag{14}$$

This section is chosen for convenience as all periodic orbits pass through it (see figure 7). For the parameters chosen here, we have $x(t-\tau) = \chi(t-\tau)$ at the switching surface. Therefore, the switching surface $\Sigma := \{h(t) = 0\}$ is orthogonal to Π in the

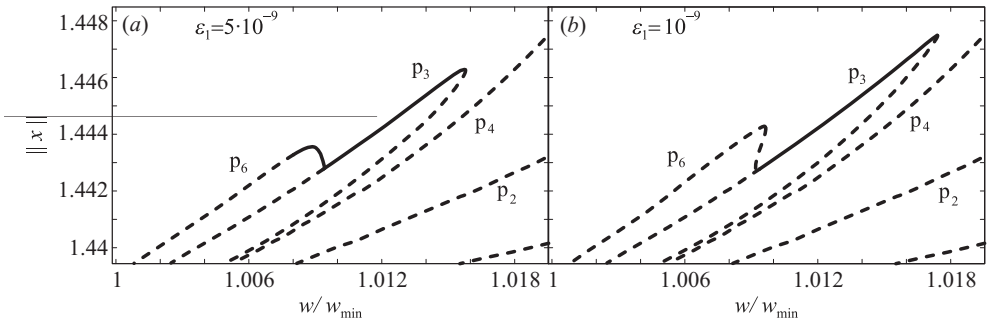

Figure 6: Panels (*a*) and (*b*) show a zoom of the marked region in figure 5(*f*) for (*a*) $\varepsilon_1 = 5 \cdot 10^{-9}$ and (*b*) $\varepsilon_1 = 10^{-9}$. The period-doubling bifurcation connecting the period-3 and period-6 branches clearly changes criticality.

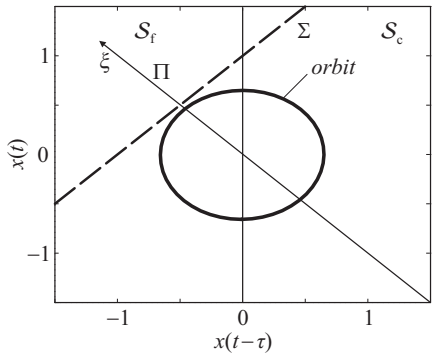

Figure 7: Shows a two dimensional projection of phase-space and a representative period-one orbit. Π marks the Poincaré section defined by (14) and Σ marks the switching surface that separates the cutting and flying vector-fields ($\mathcal{S}_c$ and $\mathcal{S}_f$).

$(x(t), x(t-\tau))$-plane and it takes the constant value of $\xi_\Sigma = 1/\sqrt{2}$. Thus, grazing bifurcations (or approximations thereof) can be immediately seen as locations where the solution branches intersect (or in the smoothed case, come close to) $\xi = \xi_\Sigma$.

At the primary grazing bifurcation (labelled B^3 in figure 8), from which many branches of periodic orbits emerge, a highly localised chaotic attractor also emerges. This chaotic attractor (cw_a) appears to be the global attractor of the system until the grazing bifurcation of the period-6 orbits (figure 8(*b*) where p_6 and p_3 were continued using $\varepsilon = 10^{-9}$). The numerical simulation also indicates that the period-3 branch continues further than the numerical continuation results show before terminating at a fold / grazing bifurcation (G_3 in figure 8(*d*)), thus extending the chaos-free window in parameter space. However, for the period-2 and period-1 branches the agreement between numerical continuation of the smoothed system and numerical simulation of the non-smooth system is excellent.

Figure 9 shows two dimensional projections of the Poincaré section defined by (14). Figures 9(*a*) and (*c*) show the phase-space when there are stable periodic orbits (solid symbols) and unstable periodic orbits (open symbols), and figures 9(*b*) and (*d*) show the phase-space when there is a stable chaotic attractor. In both cases, the agreement between simulation and continuation is good. In particular, all of the unstable periodic orbits can be seen to reside within the chaotic attractor as is expected.

5. Conclusion

This paper has been motivated by chattering behaviour in machining processes. We have focussed on a simplified one degree-of-freedom model of orthogonal cutting, as a representative example displaying the regenerative effect common to turning processes. Even this simplified modelling approach, when incorporating full chattering motions in which the tool loses contact with the workpiece, yields a non-smooth delay differential algebraic equation (DDAE) which cannot be analysed by standard numerical continuation tools.

Our chief result has been to derive a smoothed version of the orthogonal cutting system which is a pure delay differential equation (DDE) without algebraic effects. This is achieved by relaxing time to eliminate the algebraic effect, and by relaxing space to eliminate the non-smoothness that occurs at the loss of contact. These relaxations introduce two (small) smoothing parameters that govern the accuracy of the new approximate DDE system.

We have then analysed the smooth DDE system using the numerical continuation software DDE-BIFTOOL and we have compared the dynamics with initial value simulations of the full non-smooth DDAE. In broad qualitative terms, there is excellent agreement thus vindicating our approach. But the numerical continuation reveals dynamical structure and mechanisms which could not otherwise be investigated.

In particular, we have used numerical continuation to investigate the onset of chattering dynamics, at the point labelled D in figure 1(*b*). For the cubic cutting force characteristics used here, we have shown that the unstable branch of periodic orbits folds over at the same point in parameter space where its solutions first lose contact with the workpiece. This result has been suspected for some time (e.g., [15, 30]) but the matter is now resolved. However, in computations not shown here, we have discovered alternative mechanisms for the onset of chattering when other cutting force relationships are used, such as the three-quarter rule.

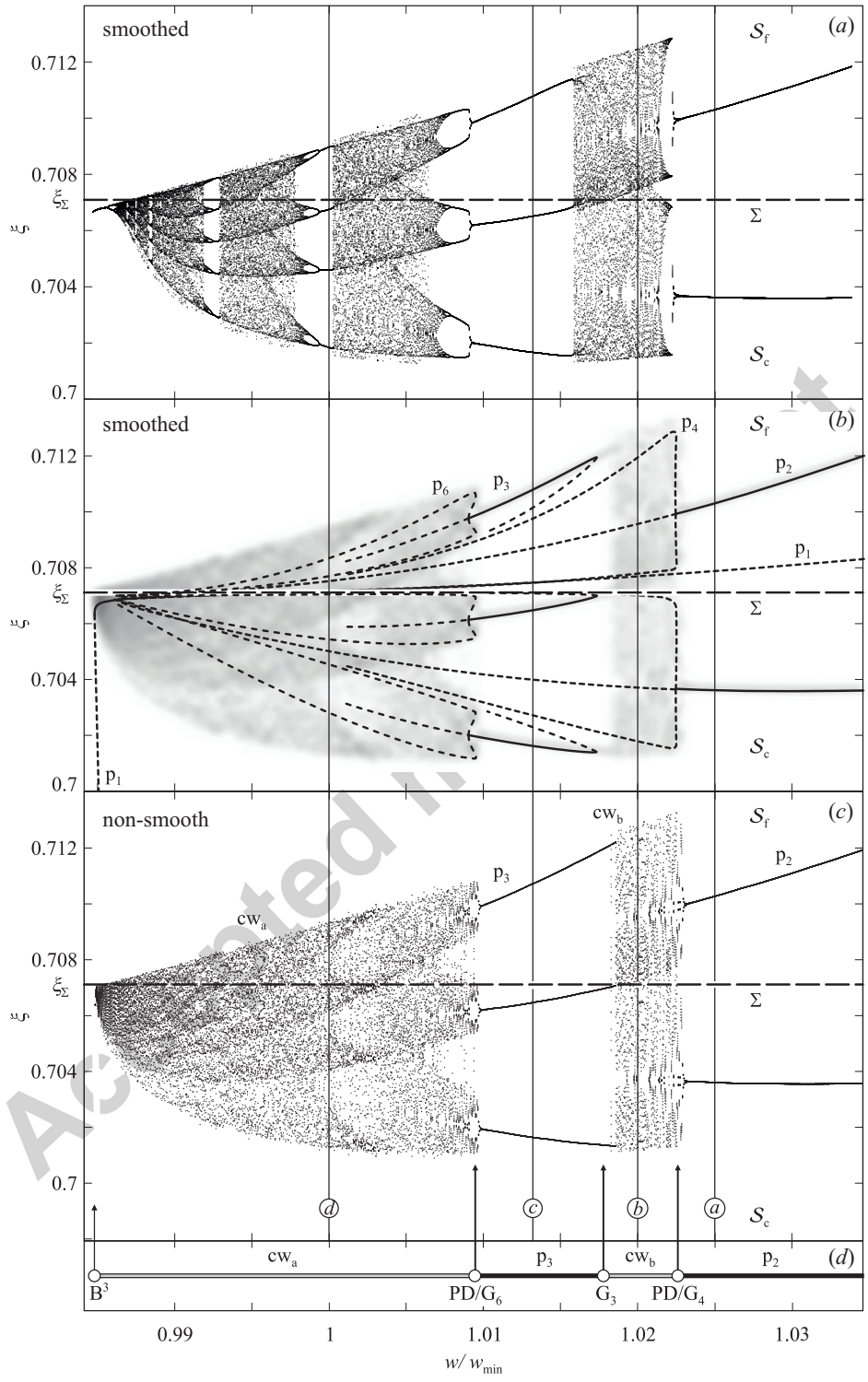

Figure 8: Panel (*a*) and (*c*) show bifurcation diagrams calculated by numerical integration of the smoothed (12) and the non-smooth model (10), respectively. Panel (*b*) contains the branches of periodic orbits obtained by numerical continuation overlaid with the results of panel (*c*) for comparison. The smoothing parameter ε_1 was $5 \cdot 10^{-9}$ in panel (*a*) and (*b*) except for branches p_3 and p_6 in panel (*b*) where ε_1 was 10^{-9}. In all panels, the vertical axis is defined by (13) in combination with the Poincaré section (14). It can be seen that a localised chaotic attractor emerges from the primary fold point / grazing (Big Bang) bifurcation B^3. Panel (*d*) shows the relative locations of the different bifurcations, where PD denotes a period-doubling bifurcation and G denotes a grazing bifurcation.

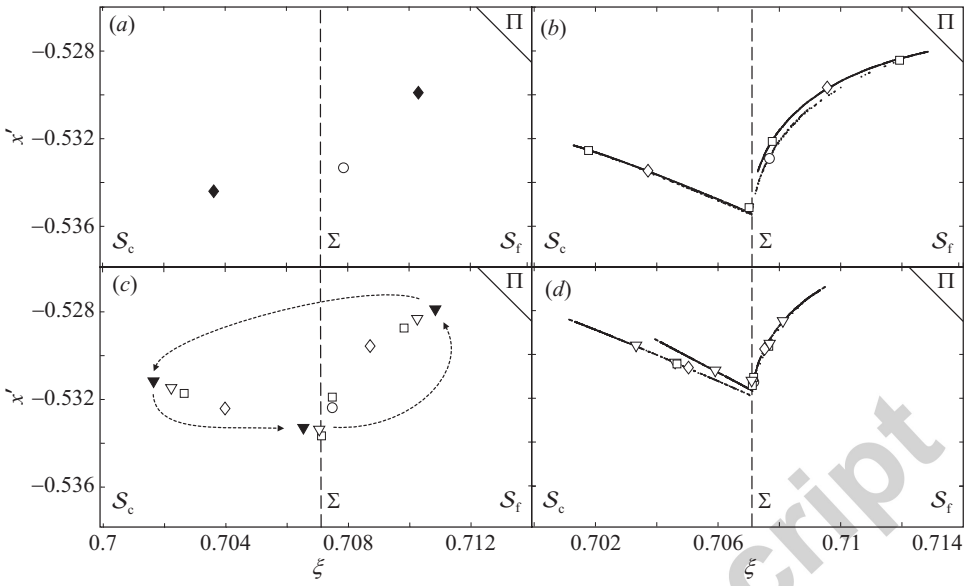

Figure 9: Two-dimensional projections of the Poincaré section (14) are shown in panels (*a*)–(*d*) corresponding to the parameter values marked in figure 8. These show the development of the bifurcation structure as the bifurcation parameter w is decreased. Panel (*a*) shows a stable period-two orbit (solid diamonds) and an unstable period-one orbit (open circle). Panel (*b*) shows a chaotic attractor with unstable period-one (open circle), period-two (open diamond) and period-four (open square) orbits. Panel (*c*) shows an example in the periodic window of figure 8 a stable period-three orbit (solid triangles), an unstable period-three orbit (open triangles) and the unstable period-one, -two and -four orbits. Panel (*d*) shows the chaotic attractor with the unstable periodic orbits embedded.

When the fine detail of solution branches is considered, some discrepancies can be found between the smoothed DDE and the full non-smooth DDAE system. Although we have established the convergence of the solution branches of the smoothed system in the limit of vanishing smoothing parameters, this converged structure is not always consistent with the DDAE in the neighbourhood of all non-smooth bifurcation points. Specifically, the route to chaos in the smoothed DDE is through a classical period-doubling cascade whereas recent parallel work has shown that the onset of chaos in the non-smooth DDAE is due to a grazing bifurcation [29]. Moreover, this grazing bifurcation (point D in figure 1(*b*)) acts as an organising centre from which all the chattering orbits emerge.

A further point to highlight is the apparent discrepancy between the results shown here and the results of Wahi and Chatterjee [31] which arises due to the use of a different cutting force model. Here the cutting rule of Shi and Tobias [13] is used whereas [31] uses the three-quarter rule [26]. When using the three-quarter rule, no chaotic chattering motion is found, only periodic motion persists. As such, further experimental work is required to determine which of the force laws is more applicable. Indeed, the results presented here may provide a distinguishing feature which can be used to differentiate between the force laws, as direct force-displacement measurements cannot be performed with sufficient accuracy. We emphasize again, however, that experimental evidence in the literature [13, 16] supports the existence of chaotic oscillations.

Finally, we should point out that our broad philosophy is focussed on detailed parameter studies of simple low degree-of-freedom models. The fine details that we discover may not survive real-world perturbations such as process damping at low spindle speeds [32] or the incorporation of higher order structural modes. However, given that very simple models display complex dynamics (including chaos) in region E, it seems plausible that the dynamics of more faithful models are at least as complicated — but their investigation remains for future work.

6. Acknowledgements

Z.D. and G.S. were supported by the Hungarian Scientific Research Foundation OTKA Grant No. K68910, HAS-BUTE Research Group on Dynamics of Machines and Vehicles, Hungarian-Spanish Intergovernmental S&T Cooperation Programme, Grant No. OMFB-01265/2007 and the OPENAER project (CENIT program of CDTI). D.A.W.B was supported by a Great Western Research fellowship. R.E.W. was supported by EPSRC grant EP/E055567/1.

References

[1] J. Tlusty, L. Spacek, Self-excited vibrations on machine tools, Nakl. CSAV, 1954, in Czech.
[2] S. Tobias, Machine-tool Vibration, Blackie, 1965.
[3] Y. Altintas, E. Budak, Analytical prediction of stability lobes in milling, CIRP Annals - Manufacturing Technology 44 (1995) 357–362.
[4] E. Budak, Y. Altintas, Analytical prediction of chatter stability in milling—part i: General formulation, Journal of Dynamic Systems, Measurement, and Control 120 (1) (1998) 22–30.

[5] S. D. Merdol, Y. Altintas, Multi frequency solution of chatter stability for low immersion milling, Journal of Manufacturing Science and Engineering 126 (3) (2004) 459–466.

[6] T. Insperger, G. Stepan, Semi-discretization method for delayed systems, International Journal for Numerical Methods in Engineering 55 (2002) 503–518.

[7] P. Bayly, J. Halley, B. Mann, M. Davies, Stability of interrupted cutting by temporal finite element analysis, Journal of Manufacturing Science and Engineering 125 (2) (2003) 220–225.

[8] M. Zatarain, J. Muñoa, G. Peigné, T. Insperger, Analysis of the influence of mill helix angle on chatter stability, CIRP Annals - Manufacturing Technology 55 (2006) 365–368.

[9] T. Insperger, D. Barton, G. Stepan, Criticality of Hopf bifurcation in state-dependent delay model of turning processes, International Journal of Non-Linear Mechanics 43 (2) (2008) 140–149.

[10] G. Litak, Chaotic vibrations in a regenerative cutting process, Chaos, Solitons & Fractals 13 (7) (2002) 1531–1535.

[11] G. Stépán, T. Kalmar-Nagy, Nonlinear regenerative machine tool vibrations, in: Proceedings of ASME Design Engineering Technical Conference, Sacramento, California, 1997, DETC97/VIB-4021.

[12] R. Szalai, G. Stépán, S. Hogan, Global dynamics of low immersion high-speed milling, Chaos 14 (4) (2004) 1069–1077.

[13] H. Shi, S. Tobias, Theory of finite-amplitude machine-tool instability, International Journal of Machine Tools and Manufacture 24 (1) (1984) 45–69.

[14] T. Kalmár-Nagy, J. Pratt, M. Davies, M. Kennedy, Experimental and analytical investigation of the subcritical instability in metal cutting, in: Proceedings of DETC'99, Las Vegas, Nevada, USA, 1999.

[15] Z. Dombóvári, R. Wilson, G. Stépán, Estimates of the bistable region in metal cutting, Proceedings of the Royal Society A: Mathematical, Physical and Engineering Science 464 (2100) (2008) 3255–3271.

[16] G. Stepan, Modelling nonlinear regenerative effects in metal cutting, Phil. Trans. R. Soc. Lond. A 359 (1781) (2001) 739–757.

[17] A. Willis, J. Peixinho, R. Kerswell, T. Mullin, Experimental and theoretical progress in pipe flow transition, Phil. Trans. R. Soc. Lond. A 366 (2008) 2671–2684.

[18] M. di Bernardo, C. Budd, A. Champneys, P. Kowalczyk, Piecewise-smooth dynamical systems: theory and applications, Vol. 163 of Applied Mathematical Sciences, Springer-Verlag, London, 2008.

[19] E. Doedel, H. Keller, J. Kernevez, Numerical analysis and control of bifurcation problems, part I, International Journal of Bifurcation and Chaos 1 (3) (1991) 493–520.

[20] E. Doedel, H. Keller, J. Kernevez, Numerical analysis and control of bifurcation problems, part II, International Journal of Bifurcation and Chaos 1 (4) (1991) 745–772.

[21] R. Seydel, Practical bifurcation and stability analysis, Springer, New York, 1994.

[22] E. Doedel, A. Champneys, T. Fairgrieve, Y. Kuznetsov, B. Sandstede, X. Wang, AUTO 97: continuation and bifurcation software for ordinary differential equations (1998).
URL `http://indy.cs.concordia.ca/auto/`

[23] A. Dhooge, W. Govaerts, Y. Kuznetsov, W. Mestrom, A. Riet, B. Sautois, MATCONT and CL_MATCONT: Continuation toolboxes in Matlab (2006).
URL `http://www.matcont.ugent.be/`

[24] K. Engelborghs, T. Luzyanina, G. Samaey, DDE-BIFTOOL v. 2.00: a Matlab package for bifurcation analysis of delay differential equations, Tech. Rep. TW330, Department of Computer Science, K.U. Leuven, Leuven, Belgium (2001).

[25] R. Szalai, PDDE-CONT: a continuation and bifurcation software for delay-differential equations (2005).
URL `http://seis.bris.ac.uk/~rs1909/`

[26] O. Kienzle, Spezifische schnittkräfte bei der metallbearbeitung, Werkstattstechnik und Maschinenbau 47 (1) (1957) 224–225.

[27] G. Stépán, Retarded dynamical systems, Longman, London, 1989.

[28] V. Avrutin, M. Schanz, On multi-parametric bifurcations in a scalar piecewise-linear map, Nonlinearity 19 (3) (2006) 531.

[29] D. Barton, Stability calculations for piecewise-smooth delay equations, International Journal of Bifurcation and Chaos 19 (2) (2009) 639–650.

[30] G. Stepan, Nonlinear Dynamics of Material Processing and Manufacturing, John Wiley & Sons, New York, 1998, Ch. Delay-differential equation models for machine tool chatter, pp. 165–192.

[31] P. Wahi, A. Chatterjee, Self-interrupted regenerative metal cutting in turning, International Journal of Non-Linear Mechanics 43 (2) (2008) 111–123.

[32] Y. Altintas, M. Eynian, H. Onozuka, Identification of dynamic cutting force coefficients and chatter stability with process damping, CIRP Annals - Manufacturing Technology 57 (1) (2008) 371–374.